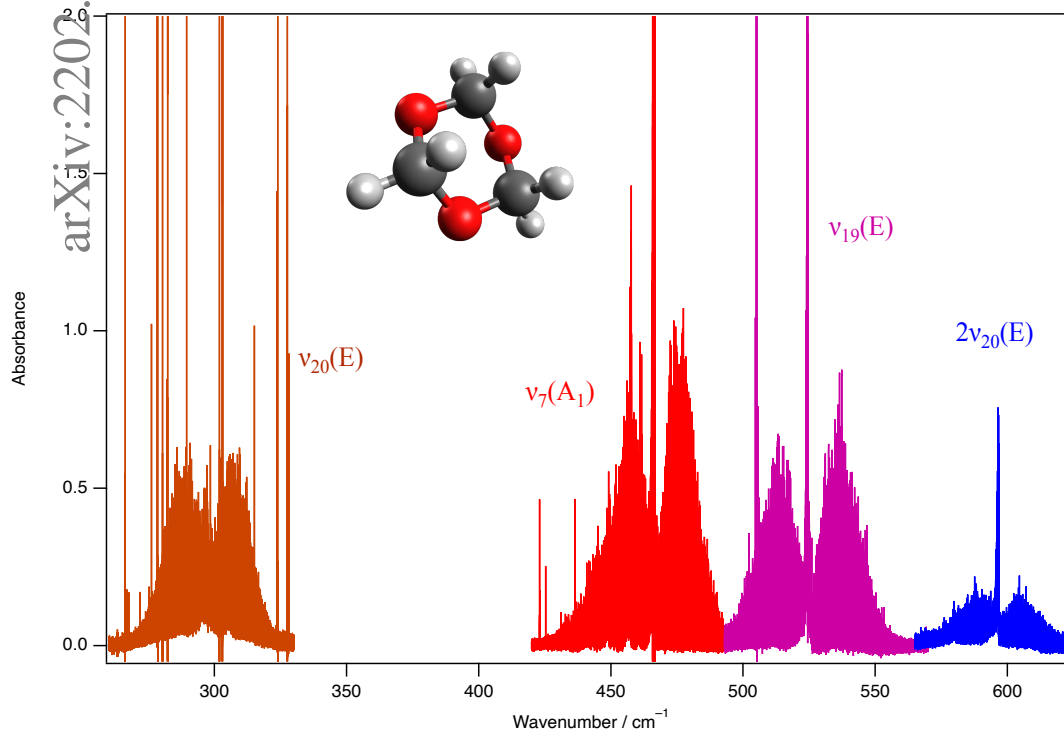


Graphical Abstract

High-resolution far-infrared synchrotron FTIR spectroscopy and analysis of the ν_7 , ν_{19} and ν_{20} bands of trioxane

C. Richard, P. Asselin, V. Boudon



Highlights

High-resolution far-infrared synchrotron FTIR spectroscopy and analysis of the ν_7 , ν_{19} and ν_{20} bands of trioxane

C. Richard, P. Asselin, V. Boudon

- Far infrared high resolution spectroscopy of four bands of the trioxane
- Complete line position analysis of ν_7 , ν_{19} and ν_{20} bands of trioxane
- Comparison of tensorial and Watson's formalism results

High-resolution far-infrared synchrotron FTIR spectroscopy and analysis of the ν_7 , ν_{19} and ν_{20} bands of trioxane

C. Richard^a, P. Asselin^b, V. Boudon^a

^a*Laboratoire Interdisciplinaire Carnot de Bourgogne, UMR 6303 CNRS - Université Bourgogne Franche-Comté, 9 Av. A. Savary, BP 47870, F-21078 Dijon Cedex, France*

^b*CNRS, De la Molécule aux Nano-Objets: Réactivité, Interactions, Spectroscopies, MONARIS, Sorbonne Université, Paris, France.*

Abstract

Rovibrational band spectra of the three ν_{20} , ν_7 and ν_{19} bands of 1, 3, 5 – trioxane (H_2CO)₃ were recorded in the 50–650 cm^{-1} range using a long path absorption cell coupled to a high resolution Fourier transform spectrometer and synchrotron radiation at the AILES beamline of the SOLEIL synchrotron. More than 16 000 lines were assigned with a dRMS better than $0.17 \times 10^{-3} \text{cm}^{-1}$. Two different formalisms (tensorial and Watson) were used to derive accurate rotational and quartic parameters for the three bands and for the first time. A precise determination of Coriolis parameter and q_+ l -doubling constant for both ν_{20} and ν_{19} perpendicular bands was also obtained. Lastly, each set of spectroscopic parameters is compared and discussed between both formalisms.

Keywords:

trioxane, high-resolution infrared spectroscopy, line positions, tensorial formalism, Watson's formalism, synchrotron radiation

1. Introduction

The molecule of 1, 3, 5 – trioxane (H_2CO)₃, a cyclic trimer of formaldehyde, is an oblate symmetric-top that belongs to the C_{3v} symmetry group as illustrated in the Fig. 1. It is a good example of a reasonably rigid molecule with 20 fundamental modes: 7 symmetric vibrations of type A_1 (parallel bands), 3 vibrations of type A_2 (for which absorption from the ground state is symmetry-forbidden) and 10 doubly degenerate vibrations of type E (perpendicular bands).

Because of its relatively high number of atoms (12) and its fairly high mass, the rotational spectrum of trioxane is dense, leading to a possible radioastronomy detection. For many years, trioxane is also known as a molecule that could be detected in comet comae[1, 2], making it as highly relevant to studies of prebiotic chemistry. Its first microwave spectrum

Email address: Cyril.Richard@u-bourgogne.fr (C. Richard)

was obtained by Oka et al.[3] in 1963, and the analysis was extended by Colmont and co-workers[4, 5, 6, 7] for the excited states below 850 cm^{-1} . Submillimetric spectra were then measured in its ground-state and its two lowest lying excited states $\nu_7 = 1$ at 467 cm^{-1} and $\nu_{20} = 1$ at 307 cm^{-1} [8]. Two jet-cooled mid-infrared spectroscopic studies reported rovibrational spectra of the ν_{17} and ν_{16} bands, respectively centered at 1071 and 1177 cm^{-1} [9].

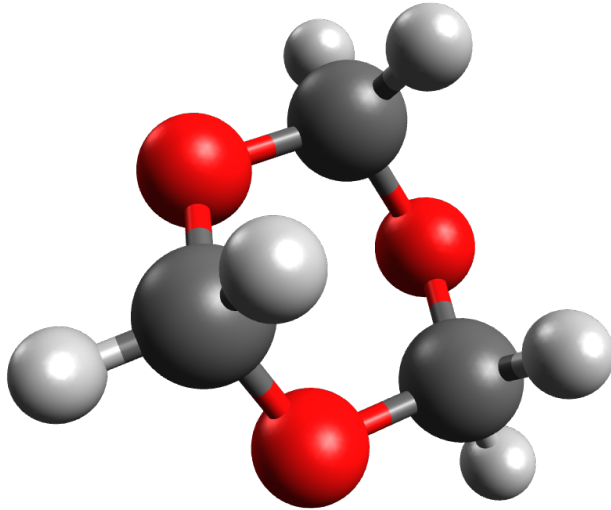


Figure 1: Three-dimensional representation of the trioxane molecule $(\text{H}_2\text{CO})_3$.

This paper presents a complete analysis of three bands, observed at high resolution in the far infrared:

- ν_{20} mode, CH_2 torsion, E , 297 cm^{-1} ,
- ν_7 mode, OCO bending, A_1 , 466 cm^{-1} ,
- ν_{19} mode, OCO bending, E , 525 cm^{-1} .

Infrared spectra of trioxane have been recorded in the $50\text{--}650\text{ cm}^{-1}$ range using a high resolution Bruker IFS 125 interferometer located at the AILES beamline of the SOLEIL synchrotron facility. Owing to its higher brilliance in the far-infrared region, the SOLEIL synchrotron radiation was used to improve the signal-to-noise ratio of the spectrum at the maximal resolution of 0.001 cm^{-1} .

The three bands were analysed independently using two different formalisms. We used in one instance Weston’s model for symmetric-top molecules, giving common spectroscopic constants, then in another instance the tensorial formulation and group theory methods developed in the Dijon group[10, 11], that allow us to provide a set of effective spectroscopic parameters. We will discuss the comparison of both models and will explain why the first overtone $2\nu_{20}$ ($A_1 + E$, 595 cm^{-1}) was measured but could not be analysed with same quality as fundamental bands.

2. Experimental details

Gas-phase trioxane ($> 99\%$, Aldrich), was injected in a multipass cell equipped with polypropylene films of $50\ \mu\text{m}$ thickness as cell windows, for which the White cell optics (White-type arrangement) were set to obtain a $150\ \text{m}$ long absorption path. The three low-frequency ν_{20} , ν_7 and ν_{19} fundamental bands of trioxane are predicted to have very different infrared intensities, respectively calculated to 0.1 , 19 and $8\ \text{km/mol}$ [12], which required us to record three spectra at different trioxane pressures to maximize absorption signal of each band: $815\ \mu\text{bar}$ for the very weak ν_{20} mode, $10\ \mu\text{bar}$ for both intense ν_7 and ν_{19} modes and $50\ \mu\text{bar}$ for the $2\nu_{20}$ overtone. The three far-IR spectra have been recorded at the maximal resolution of $0.001\ \text{cm}^{-1}$ using the SOLEIL synchrotron FIR radiation extracted by the AILES beamline as the continuum source of the FT interferometer equipped with a He-cooled bolometer detector and a $6\ \mu\text{m}$ mylar beamsplitter, resulting in a significant improvement of the signal-to-noise ratio in comparison with a global source[13, 14]. Consequently, the acquisition times for the FTIR spectra of ν_{20} , ν_7 , ν_{19} and $2\nu_{20}$ bands of trioxane were only 9 h, 11 h and 11 h30min, respectively. Both spectra were calibrated using accurate far-IR water lines absorption[15]. Thanks to the high signal-to-noise ratio obtained, the line position accuracy was estimated to $0.0002\ \text{cm}^{-1}$ for all trioxane lines observed.

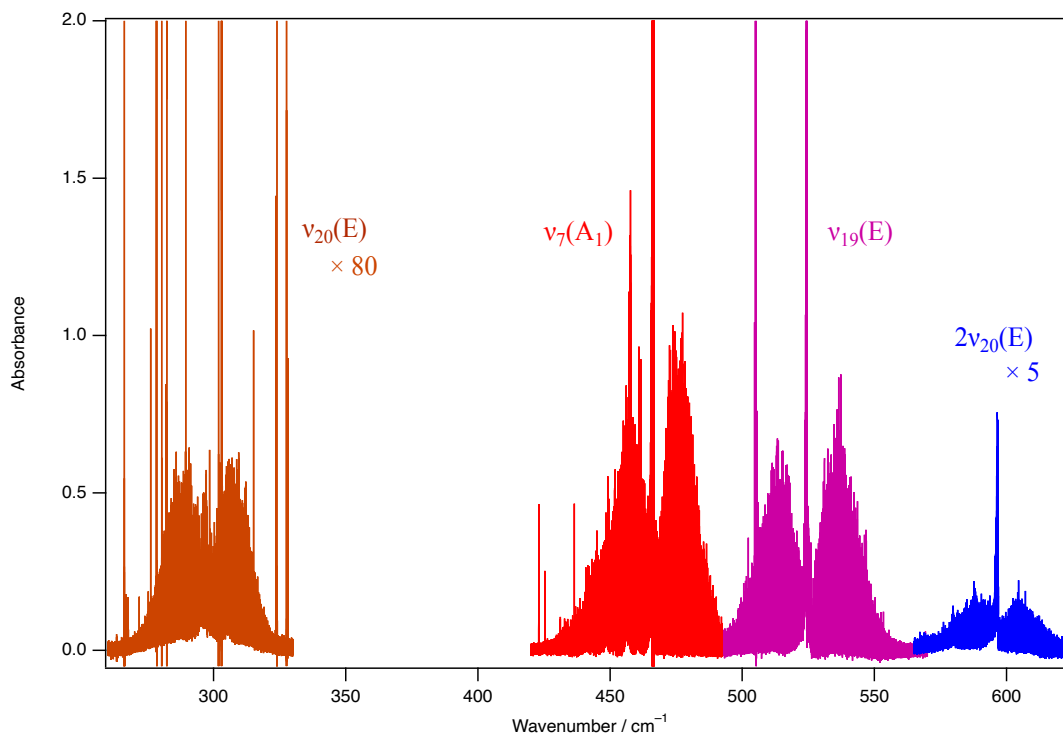


Figure 2: Overview of the high resolution spectra of the ν_{20} , ν_7 , ν_{19} and $2\nu_{20}$ bands of a sample of trioxane. The different bands were recorded at different pressure conditions, $815\ \mu\text{bar}$ for ν_{20} , $10\ \mu\text{bar}$ for ν_7 and ν_{19} and $50\ \mu\text{bar}$ for $2\nu_{20}$. The huge irregular absorption lines on the left of the spectra are water lines.

Fig. 2 displays an overview of the far-IR FT spectra of trioxane recorded at high res-

olution. The characteristic PQR band structure of three fundamentals observed is fully resolved, enabling a global rovibrational analysis. However, hot bands starting from the lowest frequency ν_{20} , ν_7 and ν_{19} modes are expected in a room temperature absorption spectrum. These features are particularly visible in the P branch of the ν_7 parallel band (Fig. 3) where two series of red shifted Q branches are observed, the first one at about 461.8, 457.2 and 452.0 cm^{-1} and tentatively assigned to $n\nu_{20} + \nu_7 \leftarrow n\nu_{20}$ transitions up to $n = 3$, the second one at 457.8 and 449.3 cm^{-1} of the type $(n + 1)\nu_7 \leftarrow n\nu_7$ up to $n = 2$ with anharmonicities estimated to $-4.8(1)$ and $-8.7(1)$ cm^{-1} , respectively. Due to the stronger density of lines in the rotational branches of perpendicular bands, hot bands are much less visible in the ν_{20} and ν_{19} spectra but their presence could be easily evidenced by subtracting the fundamental band contour simulated from the experimental ones. Consequently, the analysis of the perpendicular bands was expected to be less straightforward than the parallel one, particularly in the Q branch region due to the high density of rotational lines at high J values and the additional rotational structure of hot bands.

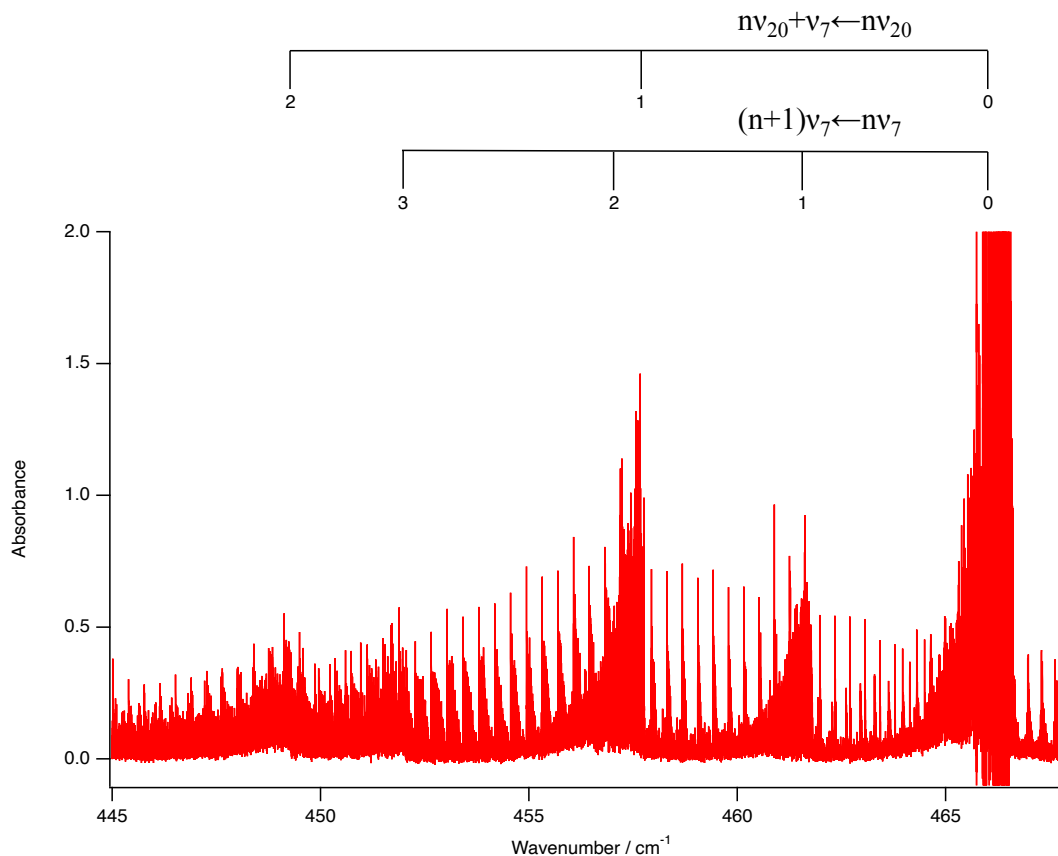


Figure 3: Two series of hot bands visible in the P branch of the ν_7 parallel branch. They have been tentatively assigned to $n\nu_{20} + \nu_7 \leftarrow n\nu_{20}$ and $(n + 1)\nu_7 \leftarrow n\nu_7$ transitions.

3. Theoretical Models

The idea of working with two different models comes from the difficulty encountered during the analysis of $2\nu_{20}$ as explained in the section 4.4. While the analysis of ν_7 , ν_{19} and ν_{20} was straightforward using Watson's formalism, the analysis of the first overtone did not yield acceptable results. Therefore, we decided to try to analyse the molecule with another model as explained below.

3.1. Tensorial formalism

Because of its high symmetry (a C_{3v} symmetric-top), trioxane is a good candidate to be analyzed by the C_{3v} Top Data System (hereafter C_{3v} TDS) software[16] developed in the Dijon group. Let us recap briefly the principles of this formalism.

The theoretical model used in C_{3v} TDS is based on the tensorial formalism and vibrational extrapolation methods described for instance in [17, 18, 19]. In the following,

- $\Gamma(= 0^+, 0^-, 1, 2, \dots)$ denotes $C_{\infty v}$ irreducibles representations (irreps),
- $C(= A_1, A_2, E)$ is used for C_{3v} irreps.

All operators are symmetrized in the $O(3) \supset C_{\infty v} \supset C_{3v}$ group chain. The $O(3)$ standard basis set $|J, M\rangle$ is oriented in the subgroups through the relation

$$|J, \Gamma, C, \sigma\rangle = \sum_{\delta=+,-} {}^{(\Gamma)}V_{C\sigma}^{\delta} \sum_{M=-\Gamma, +\Gamma} {}^{(J)}W_{\Gamma\delta}^M |J, M\rangle, \quad (1)$$

where σ is the component of C if this one is degenerate (in practice, when $C = E$). The ${}^{(J)}W_{\Gamma\delta}^M$ are given by (note that there is a phase change compared to [20]):

$$\begin{aligned} \Gamma \neq 0^{\pm} & : & {}^{(J)}W_{\Gamma\delta}^M &= \begin{cases} \frac{M}{|M|\sqrt{2}}, & \delta = +, \\ \frac{(-1)^J}{\sqrt{2}}, & \delta = -, \end{cases} \\ \Gamma = 0^{\pm} & : & {}^{(J)}W_{0^{\pm}}^M &= 1. \end{aligned} \quad (2)$$

The ${}^{(\Gamma)}V_{C\sigma}^{\delta}$ matrix elements are given in [20]. The tensorial operators are oriented in the same way.

Let us consider a molecule whose vibrational levels are grouped in a series of polyads designed by $P_k(k = 0, \dots, n, \dots)$, P_0 being the ground-state (GS). The Hamiltonian can be developed as a sum of operators specific to each polyad as:

$$\mathcal{H} = \mathcal{H}_{\{P_0=GS\}} + \mathcal{H}_{\{P_1\}} + \dots + \mathcal{H}_{\{P_k\}} + \dots + \mathcal{H}_{\{P_{n-1}\}} + \mathcal{H}_{\{P_n\}} + \dots \quad (3)$$

We can now define an effective Hamiltonian for a given vibrational polyad (or group of vibrational levels) by

$$\tilde{\mathcal{H}}^{<polyad>} = P^{<polyad>} \mathcal{H} P^{<polyad>}, \quad (4)$$

where

$$P^{<polyad>} = \sum_i |\psi_v^i\rangle\langle\psi_v^i| \quad (5)$$

is the projection operator on the vibrational Hilbert subspace, $\{|\psi_v^i\rangle\}$, for the polyad under consideration. The effective Hamiltonian for a given polyad P_n can be written as a sum of contributions of the different polyads, if the contact transformation has been built to remove inter-polyad interactions :

$$\tilde{\mathcal{H}}^{<P_n>} = \tilde{\mathcal{H}}_{\{GS\}}^{<P_n>} + \tilde{\mathcal{H}}_{\{P_1\}}^{<P_n>} + \cdots + \tilde{\mathcal{H}}_{\{P_n\}}^{<P_n>}. \quad (6)$$

The contribution of polyad P_n necessarily contains the operators and parameters of the lower polyads. The different terms are written as

$$\tilde{H} = \sum_{\text{all indexes}} \tilde{t}_{\{n_s\}\{m_s\}}^{\Omega(L,\Gamma_R)(\Gamma_1\Gamma_2\Gamma_V)\Gamma} T_{\{n_s\}\{m_s\}}^{\Omega(L,\Gamma_R)(\Gamma_1\Gamma_2\Gamma_V)\Gamma}. \quad (7)$$

All the indexes represent the intermediate quantum numbers and symmetries resulting from the construction. The \tilde{t} 's are the parameters of the model. Each T operator is constructed as a tensorial coupling between a rotational (R) and a vibrational (V) operator:

$$T_{\{n_s\}\{m_s\}}^{\Omega(L,\Gamma_R)(\Gamma_1\Gamma_2\Gamma_V)\Gamma} = \beta(R^{\Omega(L,\Gamma_R)} \otimes \varepsilon V_{\{n_s\}\{m_s\}}^{\Gamma_1\Gamma_2(\Gamma_V)})(\Gamma, A_1). \quad (8)$$

where

$$\beta = \begin{cases} \sqrt{[\Gamma_1]}(-\frac{\sqrt{3}}{4})^{\frac{\Omega}{2}} & \text{if } L = 0, \\ 1 & \text{if } L \neq 0, \end{cases} \quad (9)$$

is used to let scalar terms be equal to their equivalent in the ‘‘usual’’ non tensorial formalism [21]. $R^{\Omega(L,\Gamma_R)}$ and $\varepsilon V_{\{n_s\}\{m_s\}}^{\Gamma_1\Gamma_2(\Gamma_V)}$ are rotational and vibrational operators of respective maximum degree Ω in the rotational angular momentum components J_x , J_y and J_z and Ω_v degree in creation and annihilation vibrational operators. The order of each individual term is defined as $\Omega + \Omega_v - 2$. Let us note that here we use a coupling scheme slightly different from that of our paper [22]. *i.e.* all our couplings are made in the $C_{\infty v}$ group, then we carry out the $C_{\infty v} \supset C_{3v}$ reduction (in [22], all couplings were realized in C_{3v}).

Such a Hamiltonian development scheme enables the treatment of any polyad system. In this work and as an example, we will use the following effective Hamiltonians:

- The ground-state effective Hamiltonian

$$\mathcal{H}^{<GS>} = \mathcal{H}_{\{GS\}}^{<GS>}, \quad (10)$$

- The fundamental ν_i band effective Hamiltonian (with $i = 7, 19$ or 20 in our case)

$$\mathcal{H}^{<\nu_i>} = \mathcal{H}_{\{GS\}}^{<\nu_i>} + \mathcal{H}_{\{\nu_i\}}^{<\nu_i>}. \quad (11)$$

$H_{\{\nu_i\}}^{(\nu_i)}$ is constructed using $\varepsilon V_{\{i\}\{i\}}^{\Gamma_1\Gamma_2(\Gamma_v)}$ vibrational operators which involve creation a^+ and annihilation a operators symmetrized in $C_{\infty v}$. The rovibrational basis functions are built according to the same coupling scheme as for the operators:

$$\left| \left[\Psi_r^{(J_r, \Gamma_r)} \otimes \Psi_v^{(\{v_s\}, \Gamma_v)} \right]_{\sigma}^{(\Gamma, C)} \right\rangle, \quad (12)$$

where $\Psi_r^{(J_r, \Gamma_r)}$ is the rotational basis set and $\Psi_v^{(\{v_s\}, \Gamma_v)}$ is the vibrational one. For the twenty normal modes of vibration of trioxane, we have:

$$\Psi_v^{(\{v_s\}, \Gamma_v)} = \Psi_{v_1}^{(0^+)} \times \dots \times \Psi_{v_7}^{(0^+)} \times \Psi_{v_8}^{(0^-)} \times \Psi_{v_9}^{(0^-)} \times \Psi_{v_{10}}^{(0^-)} \quad (13)$$

$$\times \left((\dots (\Psi_{v_{11}}^{(\Gamma_{11})} \otimes \Psi_{v_{12}}^{(\Gamma_{12})})^{\Gamma_{11,12}} \otimes \dots)^{\Gamma_{11\dots 19}} \otimes \Psi_{v_{20}}^{(\Gamma_{20})} \right)^{(\Gamma_v)}. \quad (14)$$

v_1, \dots, v_{20} are vibration quantum numbers for the trioxane molecule. Γ (respectively C) is the $C_{\infty v}$ (respectively C_{3v}) total symmetry and we have the reduction:

$$\mathcal{D}^{(\Gamma)} \supset \mathcal{D}^{(C)}. \quad (15)$$

Expressions of the matrix elements of the rovibrational Hamiltonian can be easily calculated thanks to the Wigner-Eckart theorem. All the rovibrational levels are described by (J, C, α) labels where α is a numbering index for levels that have the same C_{3v} symmetry C within a J block. In this way, the usual K quantum number is hidden in the output and related to α and C symmetry. So, the K values do not appear explicitly in our labels and the ΔK nomenclature does not occur in our transition labels (although K is used internally as a $C_{\infty v}$ label).

$\mathbf{C}_{3v}\text{TDS}$ package was successfully validated in 2016 with the study of methyl iodide (CH_3I) on the band $\nu_6 = 1$, lying in the mid-infrared spectral region[23].

3.2. Watson's formalism

Defined in 1968 by James K.G. Watson in its milestone article[24], in which he simplified the vibration-rotation molecular Hamiltonian, the so-called Watsonian, is now widely used for studying polyatomic molecules.

The ro-vibrational structure of the trioxane molecule was analyzed using the following Hamiltonian:

$$\hat{H}_{\text{Watson}} = T_v + BJ(J+1) + (C-B)K^2 \quad (16a)$$

$$- D_J J^2(J+1)^2 - DJ - D_{JK} J(J+1)K^2 - D_K K^4 \quad (16b)$$

$$+ H_J J^3(J+1)^3 + H_{JK} J^2(J+1)^2 K^2 + H_{KJ} J(J+1)K^4 + H_K K^6 \quad (16c)$$

$$- 2C\zeta Kl + \eta_J J(J+1)Kl + \eta_K K^3 l \quad (16d)$$

$$+ \frac{1}{2} [q + D_{qJ} J(J+1) + D_{qK} K^2] (L_+^2 J_-^2 + L_-^2 J_+^2). \quad (16e)$$

Terms (16a), (16b) and (16c) are standard terms for symmetric-top molecules that are used for ground- and excited states. In our work, the development to the sextic constants was

needed because they have been derived in the ground state from the millimeter-wave study of Klein et al.[29]. The other terms, only appropriate for excited states, represent the Coriolis parameters (16d) and l -doubling constants (16e). Nevertheless, these are only needed for perpendicular bands. We purposely omitted here unused terms, like pure rotational C_{3v} splitting terms $\varepsilon, \varepsilon_J, \dots$, that were not fitted in the present study.

3.3. Conversion between both formalisms

Although the two models are different, they are both built on the same general principles. It is thus possible to convert spectroscopic parameters from one formalism to another. This is done by expanding both the Watsonian and our tensorial Hamiltonian in terms of elementary rotational operators J^+ , J^- and J_z and then by identifying the coefficients of each term. In practice, this is performed thanks to the Maxima symbolic computation software[25]. In this section, we will list the resulting formulas needed to convert tensorial parameters to Watsonian parameters (and vice versa) in the case of the trioxane molecule. Further details on how these formulas were determined are described in another publication[26] in the case of purely rotational operators. Coriolis (ζ , η_J) and l -doubling constants (q_+) are derived by comparing the eigenvalues of the corresponding operators in both models. η_K is not so straightforward because parameter $t_i^{3(3,S^-)}$ is a more complex combination of Coriolis and higher order l -doubling constants like $t_i^{4(2,D)}$, so its expressions requires a complete analytical development of ro-vibrational operator that will be attempted in the near future.

3.3.1. Tensorial to Watson

The Watson's parameters used in our fit (except η_K , see above), in terms of tensorial parameters:

$$\left\{ \begin{array}{l}
 B = -\frac{3 \cdot 2^{\frac{7}{2}} t_i^{4(4,S^+)}}{\sqrt{35}} - \frac{2^{\frac{3}{2}} t_i^{2(2,S^+)}}{\sqrt{3}} + t_i^{2(0,S^+)}, \\
 C = \frac{19 \cdot 2^{\frac{5}{2}} t_i^{4(4,S^+)}}{\sqrt{35}} + \frac{2^{\frac{5}{2}} t_i^{2(2,S^+)}}{\sqrt{3}} + t_i^{2(0,S^+)}, \\
 D_J = -\frac{32 \sqrt{6} t_i^{6(4,S^+)}}{\sqrt{35}} - \frac{3 \cdot 2^{\frac{5}{2}} t_i^{4(4,S^+)}}{\sqrt{35}} - \frac{2^{\frac{7}{2}} t_i^{4(2,S^+)}}{3} - t_i^{4(0,S^+)}, \\
 D_{JK} = \frac{8 \cdot 10^{\frac{3}{2}} t_i^{6(4,S^+)}}{\sqrt{21}} + \frac{24 \sqrt{10} t_i^{4(4,S^+)}}{\sqrt{7}} + 2^{\frac{7}{2}} t_i^{4(2,S^+)}, \\
 D_K = -4 \sqrt{70} t_i^{4(4,S^+)}, \\
 \zeta = -\frac{t_i^{1(1,S^-)}}{C \sqrt{2}}, \\
 \eta_J = 4 \sqrt{\frac{2}{3}} t_i^{3(1,S^-)}, \\
 q_+ = 2 t_i^{2(2,D)}, \\
 H_J = -\frac{16 \sqrt{6} t_i^{6(4,S^+)}}{\sqrt{35}} - \frac{2^{\frac{11}{2}} t_i^{6(2,S^+)}}{3^{\frac{3}{2}}} + t_i^{6(0,S^+)}, \\
 H_{JK} = \frac{32 \sqrt{30} t_i^{6(4,S^+)}}{\sqrt{7}} + \frac{2^{\frac{11}{2}} t_i^{6(2,S^+)}}{\sqrt{3}}, \\
 H_{KJ} = -\frac{16 \sqrt{70} t_i^{6(4,S^+)}}{\sqrt{3}}.
 \end{array} \right. \quad (17)$$

3.3.2. Watson to tensorial

Expression of tensorial parameters used in our fit, in terms of Watson's parameters, without $t_i^{3(3,S^-)}$ and $t_i^{4(2,D)}$ (see the explanation at the beginning of Sect. 3.3) are:

$$\left\{ \begin{array}{l} t_i^{1(1,S^-)} = -\zeta C \sqrt{2}, \\ t_i^{2(0,S^+)} = \frac{D_K}{15} + \frac{2B}{3} + \frac{C}{3}, \\ t_i^{2(2,S^+)} = \frac{5D_K}{14\sqrt{6}} - \frac{B}{2\sqrt{6}} + \frac{C}{2\sqrt{6}}, \\ t_i^{2(2,D)} = \frac{q_+}{2}, \\ t_i^{3(1,S^-)} = \eta_J \frac{\sqrt{3}}{4\sqrt{2}}, \\ t_i^{4(0,S^+)} = -\frac{H_{KJ}}{15} - \frac{D_K}{5} - \frac{D_{JK}}{3} - D_J, \\ t_i^{4(2,S^+)} = \frac{5H_{KJ}}{7 \cdot 2^{\frac{7}{2}}} + \frac{3D_K}{7 \cdot 2^{\frac{5}{2}}} + \frac{D_{JK}}{2^{\frac{7}{2}}}, \\ t_i^{4(4,S^+)} = -\frac{D_K}{4\sqrt{70}}, \\ t_i^{6(0,S^+)} = \frac{H_{KJ}}{5} + \frac{H_{JK}}{3} + H_J, \\ t_i^{6(2,S^+)} = \frac{3^{\frac{3}{2}} H_{KJ}}{7 \cdot 2^{\frac{9}{2}}} + \frac{\sqrt{3} H_{JK}}{2^{\frac{11}{2}}}, \\ t_i^{6(4,S^+)} = -\frac{\sqrt{3} H_{KJ}}{16\sqrt{70}}. \end{array} \right. \quad (18)$$

The Dijon tensorial model relies on the so-called ‘‘vibrational extrapolation’’ (see Eq. 6) that possesses a clear advantage to ensure the convergence of fits and consistency of parameters. In practice, this means that effective Hamiltonian parameters for a given vibrational state or polyads are (presumably small) corrections to the parameters of the states (or polyads) below. Just as a simple illustration, we can say that the traditional approach consists in fitting parameters for each state: $B_0, D_0, \dots, B_1, D_1, \dots$. The vibrational extrapolation methods rather consists in fitting $B_0, D_0, \dots, \Delta B_1 = B_1 - B_0, \Delta D_1 = D_1 - D_0, \dots$. Ensuring that parameter values for each state are not too far from the ground state ones amounts to verify that $\Delta B_1 = B_1 - B_0, \Delta D_1 = D_1 - D_0, \dots$ are small. Fixing these difference to zero, like $\Delta D_1 = 0$ for instance forces excited state parameters to be identical to the ground state ones in the fit when such a constraint appears necessary.

This principle is applied in the present study. Thus, for the connection with Watson's formalism, in order to apply the conversion formulas, we first started to convert our ‘‘difference’’ excited state parameters, let us call them Δt_i^k ($i = 7, 19$ or 20 , and k the parameter index representing $\Omega(L, \Gamma_R)$) to an ‘‘absolute’’ excited state value by adding the ground state value ($t_i^k = \Delta t_i^k + t_0^k$, were t_0^k is a ground-state parameter). Then, the conversion formulas

give Watsonian parameters for state i , like B_i , *etc.* Of course, some excited state parameters like Coriolis ones have no counterpart in the ground state and are thus not differences but directly “absolute” excited state values.

In the case of fundamental excited states ($v = 1$) with E symmetry (ν_{19} and ν_{20} in our case), all Δt_i^k have to be multiplied by the matrix element of the vibrational operator, which is $1/\sqrt{2}$ and, when $L = 0$, one also has to take into account the $\sqrt{[\Gamma_1]} = \sqrt{2}$ factor which is present in the β factor (see Eqs. (8) and (9) above). The general conversion formulas for any vibrational state will be the subject of a future paper.

4. Analysis and discussion

Spectra analyses were conducted with different software packages. First, for the tensorial formalism, we used the software suite developed in the Dijon group ; SPVIEW (Spectrum-View)[11], in its version 2.0¹, for the line assignment and XTDS (eXtended spherical-Top Data System)[11], using C_{3v} TDS package, for spectra modeling and job executions. Then, for Watson’s formalism, we used the well known PGOPHER[27], program for rotational, vibrational and electronic spectra developed by the late Dr Colin Western and SPFIT[28], the program of H.M. Pickett originally written to fit and predict spectra of asymmetric-top molecules involving spin- and rotation-vibration interaction and treating symmetric-top ones as special cases.

Fig. 4 compares experiment and simulation for the ν_7 band. Some insets show again that the fine structure is very well modeled.

4.1. Analysis in the tensorial formalism

This analysis takes advantage of the millimeter-wave study of Klein *et al.*[29] in the ground-state region around 350–950 GHz. Data from the paper were converted into a 2-columns flat file in order to produce a stick spectrum readable by SPVIEW. Then, we proceeded to a line assignment to perform a standard iterative Levenberg-Marquardt non-linear least squares fit. A total of 289 lines (218 different frequencies) were used, giving a root mean square deviation of 0.015 MHz with eight parameters up to the sixth order (six free and two fixed), as shown in Table 1. As pure rotational data for only one isotopologue do not allow us to fit C and D_K , the molecule’s structure remains undetermined. These parameters were derived from a study of Colmont[30] in 1974 thanks to ¹³C and ¹⁸O isotopic substitutions, which break the molecular. On our side, all ground-state parameters were used in the formulas (18) as a starting point of our fit and the two spectroscopic parameters $t_i^{2(2,S^+)}$ and $t_i^{4(2,S^+)}$ were fixed to the calculated value.

The ν_7 , ν_{19} and ν_{20} bands were analysed successively, first by manually estimating the band center and using rotation constants from ground-state in order to produce a fit and a first prediction. Then, the fit was iteratively improved, releasing more parameters, by adding new identified lines.

¹<https://icb.u-bourgogne.fr/spview>

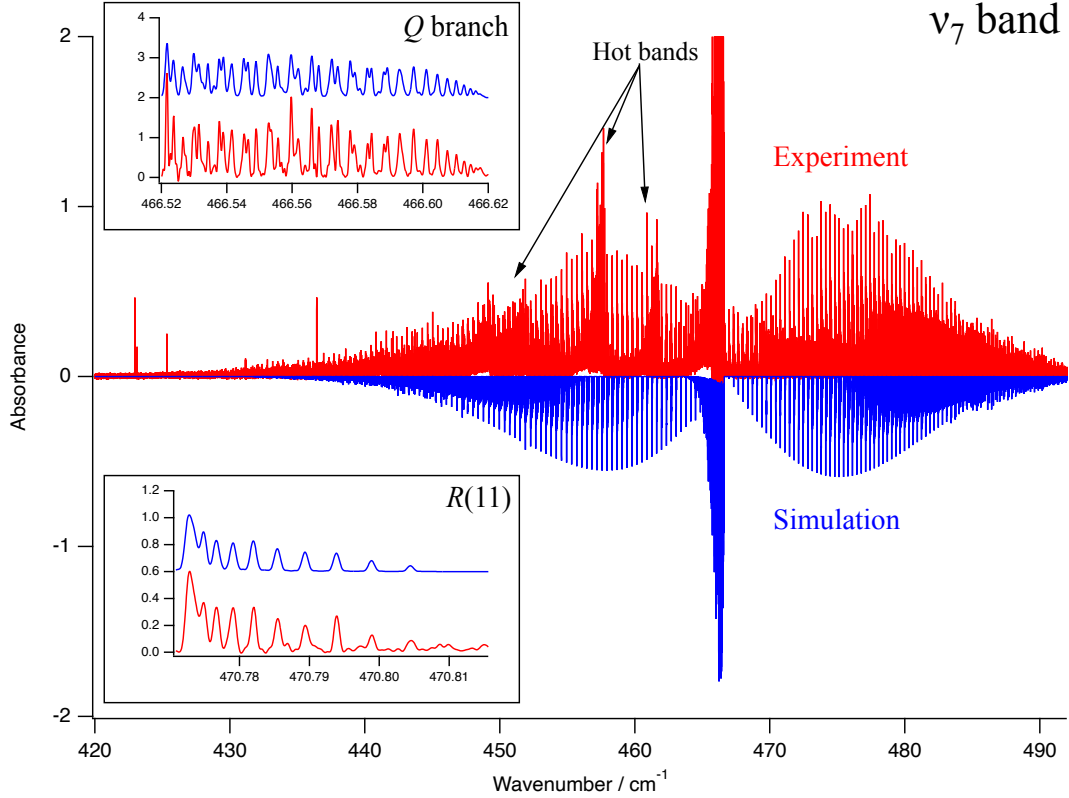


Figure 4: The ν_7 band, compared to the simulation. The insets display a few lines in the Q branches and the K series in $R(11)$.

Then, we performed a global fit using a dedicated polyad scheme where P_0 is the ground-state, $P_3 - P_0$ stands for the ν_{20} band, $P_4 - P_0$ for ν_7 and $P_5 - P_0$ for ν_{19} . In this scheme it is possible to add the first overtone of ν_{20} in $P_6 - P_0$. We obtained an excellent fit whose root mean squares deviation are 0.015 MHz , $1.32 \times 10^{-4} \text{ cm}^{-1}$, $1.38 \times 10^{-4} \text{ cm}^{-1}$ and $1.63 \times 10^{-4} \text{ cm}^{-1}$ for the transitions GS–GS, ν_7 –GS, ν_{19} –GS and ν_{20} –GS, respectively. The global standard deviation is of 0.245 for a total of 16 320 lines. Fig. 5 details the fit residuals for line positions for these four types of transitions, along with some statistics, then all the fit results are gathered in Table 1.

Finally, $t_i^{4(2,D)}$, $t_i^{4(4,D)}$ and $t_i^{5(1,S^-)}$ are fitted in the ν_{19} band, but not in the ν_{20} . Indeed, adding these parameters to the latter does not improve the fit and they are not well defined. In the same way, removing them from the ν_{19} one degrades the fit by a factor 11.

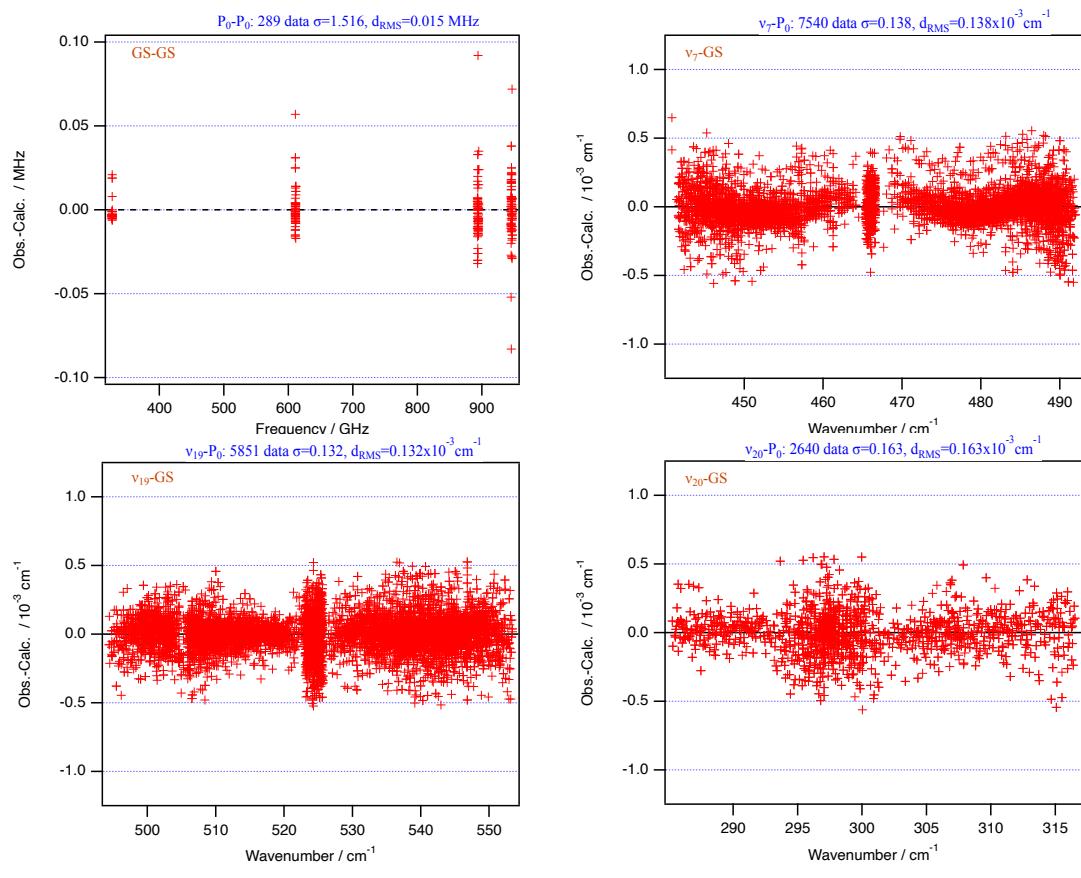


Figure 5: Fit residuals for line positions for the rotational and the three different types of ro-vibrational transitions used in the present work.

Table 1: Spectroscopic constants of the ground-vibrational state, ν_7 , ν_{19} and ν_{20} bands of Trioxane fitted in the tensorial formalism.

Parameters	Value / cm^{-1} (Hamiltonian \tilde{H})			
	GS	ν_7	ν_{19}	ν_{20}
$t_i^{0(0,S^+)}$		466.618966(37)	524.466369(30)	297.703777(50)
$t_i^{1(1,S^-)}$			9.25909(12) $\times 10^{-2}$	3.91660(11) $\times 10^{-2}$
$t_i^{2(0,S^+)}$	1.498526396(12) $\times 10^{-1}$	-3.46744(31) $\times 10^{-4}$	4.7671(27) $\times 10^{-5}$	-1.38378(70) $\times 10^{-4}$
$t_i^{2(2,S^+)}$	-1.5948802396 [†] $\times 10^{-2}$	5.3640(12) $\times 10^{-5}$	-6.4955(13) $\times 10^{-5}$	2.7883(31) $\times 10^{-5}$
$t_i^{2(2,D)}$			-2.16888(36) $\times 10^{-4}$	-1.29879(74) $\times 10^{-4}$
$t_i^{3(1,S^-)}$			4.060(27) $\times 10^{-8}$	2.288(15) $\times 10^{-8}$
$t_i^{3(3,S^-)}$			-1.018(14) $\times 10^{-8}$	-8.65(12) $\times 10^{-9}$
$t_i^{4(0,S^+)}$	-2.357311(25) $\times 10^{-8}$	1.2388(57) $\times 10^{-9}$	-7.470(53) $\times 10^{-10}$	1.32(23) $\times 10^{-10}$
$t_i^{4(2,S^+)}$	-5.5033842448 [†] $\times 10^{-9}$	2.262(12) $\times 10^{-10}$	-1.454(14) $\times 10^{-10}$	4.23(60) $\times 10^{-11}$
$t_i^{4(2,D)}$			-5.064(40) $\times 10^{-10}$	
$t_i^{4(4,S^+)}$	-1.74069(41) $\times 10^{-10}$	6.138(47) $\times 10^{-11}$	-4.658(52) $\times 10^{-11}$	1.84(19) $\times 10^{-11}$
$t_i^{4(4,D)}$			-1.016(52) $\times 10^{-10}$	
$t_i^{5(1,S^-)}$			-1.38(12) $\times 10^{-13}$	
$t_i^{6(0,S^+)}$	1.1285(18) $\times 10^{-14}$			
$t_i^{6(2,S^+)}$	3.146(20) $\times 10^{-16}$			
$t_i^{6(4,S^+)}$	-1.17956(68) $\times 10^{-15}$			
Lines fitted	289	5851	7540	2640
J_{max}	89	80	90	88
free parameters	6	6	13	10
d_{RMS}^*	0.015	0.132	0.138	0.163
Total of Lines	16 320			
Standard deviation	0.245			

* d_{RMS} is given in 10^{-3}cm^{-1} except GS that is in MHz.

[†] Fixed value.

4.2. Analysis in the Watson formalism

Preliminary simulations of the three far-IR bands of trioxane were carried out separately using PGOPHER program configured with the Watson’s Hamiltonian dedicated to oblate top-symmetric molecules. The rovibrational analysis of the ν_7 OCO bending mode (A symmetry) centered at about 466 cm^{-1} is realized on grounds of a parallel band using only (16a), (16b) and (16c) standard terms of \hat{H}_{Watson} . For both ν_{20} CH₂ torsion and ν_{19} OCO bending modes (E symmetry) centered at about 297 and 524 cm^{-1} , the presence of Coriolis parameters and l -doubled states requires to use (16d) and (16e) non standard terms. The fit of each band is realized by fixing the ground state constants to Klein et al values and excited state sextic constants to ground state ones. At low values of J , K , only the band center and two rotational constants are adjusted for a parallel band to which the ζ Coriolis and q_+ l -doubling parameter are added for a perpendicular band. At higher values of J , K , quartic constants and higher order of ζ and q_+ terms are introduced.

The three linelists obtained from the PGOPHER simulations are then converted in a single .lin file to realize a global adjustment of ν_7 , ν_{19} and ν_{20} , bands with the SPFIT program. For this last step, the 213 millimeter-wave lines of Klein et al. are added to the excited state line transitions so that ground- and excited-state parameters are together adjusted.

We obtained a root mean squares deviation of $1.17 \times 10^{-4}\text{ cm}^{-1}$, $2.52 \times 10^{-4}\text{ cm}^{-1}$ and $1.56 \times 10^{-4}\text{ cm}^{-1}$ for the transitions ν_7 -GS, ν_{19} -GS and ν_{20} -GS, respectively. The global standard deviation is of 0.609 for a total of 15 512 lines. Fig. 6 details the fit residuals for line positions for these 3 transitions, along with some statistics while the spectroscopic parameters are gathered in Table 2.

Table 2: Spectroscopic constants of the ground-vibrational state, ν_7 , ν_{19} and ν_{20} bands of Trioxane. These parameters were determined in the Watsonian formalism using SPFIT program.

Parameters	GS	ν_7	ν_{19}	ν_{20}
T_v (cm ⁻¹)		466.618 962(12)	524.466 456(15)	297.703 913(16)
B (MHz)	5273.257 177(41)	5260.235 81(41)	5276.946 22(73)	5268.150 03(82)
C (MHz)	2933.95(27)	2928.81(27)	2930.89(27)	2931.73(27)
D_J (kHz)	1.343 889 7(92)	1.275 86(10)	1.392 20(28)	1.342 95(28)
D_{JK} (kHz)	-2.016 344(20)	-1.886 96(23)	-2.105 56(59)	-2.011 70(60)
D_K (kHz)	0.17 [‡]	0.108 83(16)	0.218 42(33)	0.166 27(35)
ζ			-0.668 69(15)	-0.282 15(10)
η_J (kHz)			-2.311(8)	-0.922(10)
η_K (kHz)			-3.037(8)	-2.249(10)
q_+ (MHz)			12.9115(12)	7.6313(31)
H_J (mHz)	0.491 38(60)	0.491 38 [†]	0.491 38 [†]	0.491 38 [†]
H_{JK} (mHz)	-2.0993(14)	-2.0993 [†]	-2.0993 [†]	-2.0993 [†]
H_{KJ} (mHz)	2.7352(19)	2.7352 [†]	2.7352 [†]	2.7352 [†]
Lines fitted	212	6405	4894	4005
J_{\max}	89	80	99	91
free parameters	7	6	10	10
d_{RMS}^*	0.011	0.117	0.252	0.156
Total of Lines	15 512			
Standard deviation	0.609			

* d_{RMS} is given in 10⁻³cm⁻¹ except GS that is in MHz.

[‡] Ground-state parameters fixed to the value of Klein *et al.* [29].

[†] ν_7 , ν_{19} and ν_{20} sextic parameters are fixed to the ground-state values..

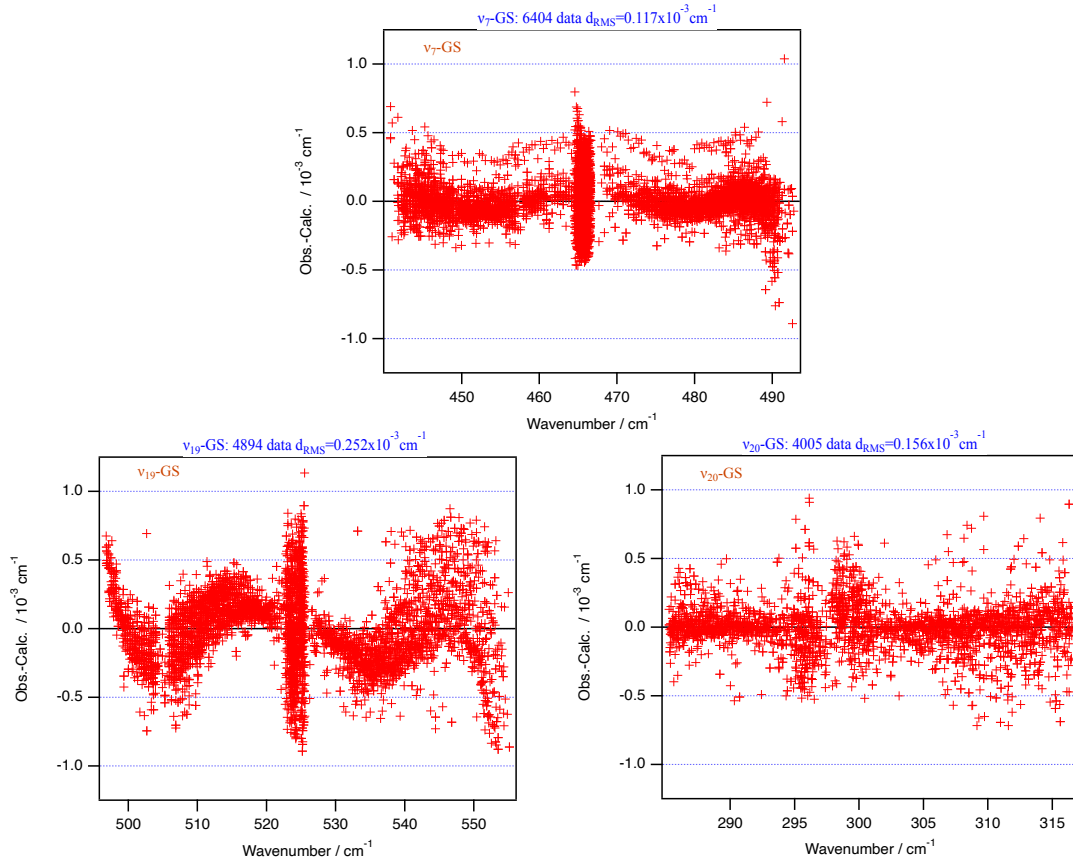


Figure 6: Fit residuals for line positions for the three different types of ro-vibrational transitions used in the present work, with the Watson’s formalism.

4.3. Comparison of both formalisms

Thanks to the formulas transcribed in Sect. 3.3.1, we report the Watsonian spectroscopic constants converted from the tensorial ones in Table 4. This allows an easier comparison between the two models. In this section, we will detail each parameter and examine the differences we observe.

First of all, not all spectroscopic constants have been converted because some of them have no equivalence in the fit we have provided in Sect. 4.2. It is the case for $t_i^{3(3,S^-)}$ as already explained in Sect. 3.3 and for $t_i^{5(1,S^-)}$ which is a Coriolis parameter at higher order than η_J . Then, the two parameters $t_i^{4(2,D)}$ and $t_i^{4(4,D)}$ represent the centrifugal distortion of q_+ l doubling constant, called D_{qJ} and D_{qK} in Eq. (16) but not fitted in this study with the Watson’s model.

Second, sextic parameters are all together fixed to the values fitted for the ground-state. This is simply because no sextic parameters were fitted for the excited states in our tensorial model, as stated in Sect. 3.3.2. Regarding the residuals in Fig. 6, $\nu_{19} - \text{GS}$ is less good than the ones obtained with the other formalism in Fig. 5 and a polynomial shape is visible in

the obs.–calc. plot. The fit could be improved by releasing sextic parameters, however the constants thus derived have values that look spurious, and far from those of the GS. We therefore decided to keep the results consistent for a better comparison of the models.

About rotational constants, the comparison between both formalisms of two K –dependent terms, namely $(\Delta C - \Delta B)K^2$ and $-2C\zeta K$ shows a fair agreement for the parallel band ν_7 (only the term in K^2 exists) with $(\Delta C - \Delta B)K^2$ equal to of 7.8781 and 7.8788 MHz for TDS and Watson formalisms, respectively. For the perpendicular bands ν_{19} and ν_{20} , we have illustrated in Table 3 the slight differences between the K –dependent terms for different values of K . The sum of two terms differs by about 60 and 500 MHz between TDS and Watson formalisms for K equal to 10 and 80, respectively. The term $-2C\zeta K$ is mainly responsible for this variation as indicated on Table 3. Knowing that the agreement between both formalisms is excellent for the Coriolis parameter (only 0.3% variation for both bands), the main difference may come only from the value of C in the ground state: in the Watsonian fit, C is fixed to 2933.95 cm^{-1} [30] while in the tensorial fit, the iterative fit detailed in Sect. 4.1 imposes that C in the ground state is adjusted as all other ground and excited state parameters. The difference of about 3 MHz between both values of C leads to a difference of about 300 and 150 MHz at $K = 80$ for $-2C\zeta K$, respectively for ν_{19} and ν_{20} .

Table 3: Comparison between rotational constants for ν_{19} and ν_{20} and formalisms. For each K the first line gives the value of the expression $(\Delta C - \Delta B)K^2$, while the second one is the result of $-2C\zeta K$. Values are given in MHz.

K	Tensorial		Watson	
	ν_{19}	ν_{20}	ν_{19}	ν_{20}
1	−6.746	2.896	−6.755	2.889
	3925.582	1660.523	3919.740	1654.376
10	−674.575	289.565	−675.522	288.883
	39 255.816	16 605.232	39 197.407	16 543.763
50	−16 864.375	7239.125	−16 888.050	7222.075
	196 279.079	83 026.158	195 987.036	82 718.816
80	−43 172.800	18 532.160	−43 233.408	18 488.512
	314 046.526	132 841.853	313 579.258	132 350.105

The l –doubling constant q_+ well agrees between them for both ν_{19} and ν_{20} bands (1.4% variation in average). Nevertheless, values given in the publication of Oka et al. [3] ($q_+(\nu_{19}) = 7.50$ and $q_+(\nu_{20}) = 12.60$) seem to be swapped with regards to this work.

Finally, regarding the parameter η_J , that represent the $J(J + 1)$ dependence of Coriolis coupling constant, we report a mismatch in the two E bands that can be explained by the fact that higher order parameters are used in tensorial formalism; as a consequence, comparison has little meaning here.

Table 4: Spectroscopic constants of the ground-state and the three ground-vibrational state, ν_7 , ν_{19} and ν_{20} bands of Trioxane. These values were obtained from the tensorial formalism and converted to the Watsonian. As explained in Sect. 3.3.2, to apply the conversion formulas, ground state value is added to the excited state parameters ($t_k^i = \Delta t_k^i + t_0^k$).

Parameters	GS	ν_7	ν_{19}	ν_{20}
T_v (cm ⁻¹)		466.618 966(37)	524.466 369(30)	297.703 777(50)
B (MHz)	5273.257 035(36)	5260.2359(11)	5276.2202(6)	5270.2176(15)
C (MHz)	2930.892 885(36)	2925.7498(15)	2927.1103(10)	2930.7491(24)
D_J (kHz)	1.343 880(11)	1.275 89(23)	1.369 534(43)	1.337 40(17)
D_{JK} (kHz)	-2.016 314(48)	-1.886 81(16)	-2.079 51(49)	-1.9950(19)
D_K (kHz)	0.174 643(41)	0.113 06(51)	0.207 69(41)	0.1616(14)
ζ			-0.670 555 8(12)	-0.283 293 3(11)
η_J			-3.9752(81)	-2.2402(45)
q_+			13.0043(11)	7.7873(22)
H_J (mHz)	0.490 44(76)	0.490 44 [†]	0.490 44 [†]	0.490 44 [†]
H_{JK} (mHz)	-2.0962(21)	-2.0962 [†]	-2.0962 [†]	-2.0962 [†]
H_{KJ} (mHz)	2.7331(16)	2.7331 [†]	2.7331 [†]	2.7331 [†]

[†] ν_7 , ν_{19} and ν_{20} sextic parameters are fixed to the ground-state values.

4.4. The first overtone $2\nu_{20}$

The $2\nu_{20}$ band, centered around 595 cm^{-1} , is composed of a parallel sub-band (A_1) and a perpendicular sub-band (E) very close in energy as illustrated in Fig. 7. The E sub-band is less intense but Q branches are clearly visible for both sub-bands. Using parameters fitted for ν_{20} as a starting point of a new fit gives a prediction that seems close in a first look. Nevertheless, while line assignment in the A_1 sub-band seems to be not too difficult thanks to the fair enough signal intensity, it is not the same for the other.

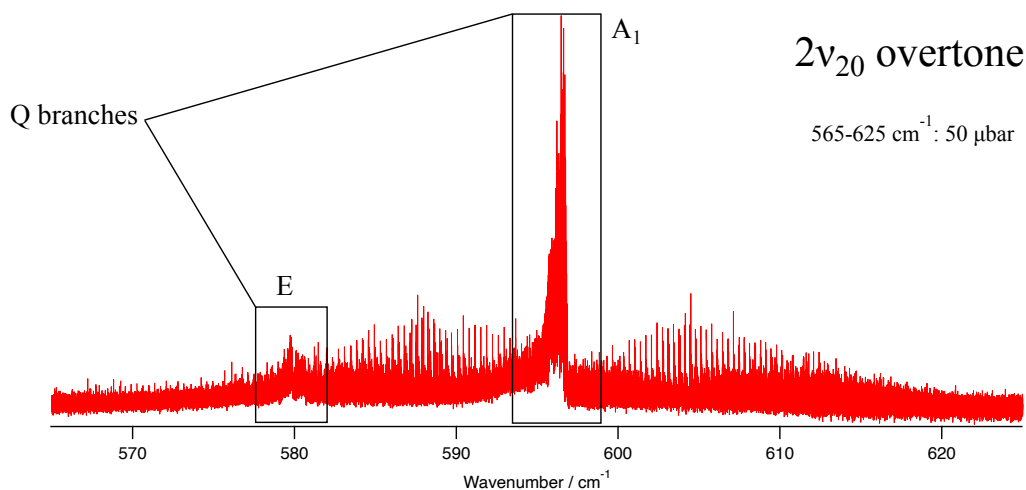


Figure 7: Part of the spectrum showing the first overtone $2\nu_{20}$ composed of a parallel band and a perpendicular band very close in energy. While the shape of the two Q branches is visible, the perpendicular band has a poor signal-to-noise ratio and shows a very strong perturbation.

Attempts have been made to fit data iteratively as it was done for other bands. Nevertheless, even if the line pattern is clearly visible, perturbations quickly grow as K value does, as illustrated in Fig. 8. Analysis of A_1 - and E - level interaction is then needed but the signal-to-noise ratio is not good enough for the E sub-band and assignment is not possible so far. As a consequence, A_1 sub-band cannot be analyzed in its entirety, especially for high K values, since we cannot characterise interaction with the E sub-level. Recording another spectrum with a longer optical path could help to fix this issue. The analysis of the $2\nu_{20} \leftarrow \nu_{20}$ hot band, observed along with the $\nu_{20} \leftarrow 0$ fundamental transition could enable to assign unambiguously many $\nu_{20} = 2$ rovibrational states and untangle this overtone analysis.

5. Conclusion

Ro-vibrational spectra were analysed in the laboratory for the three bands ν_7 , ν_{19} and ν_{20} bands of the trioxane molecule. We could determine with accuracy a set of spectroscopic constants derived from Watson's and tensorial formalism for C_{3v} molecules developed in the Dijon group. This study allowed us to compare results from both models in a reliable

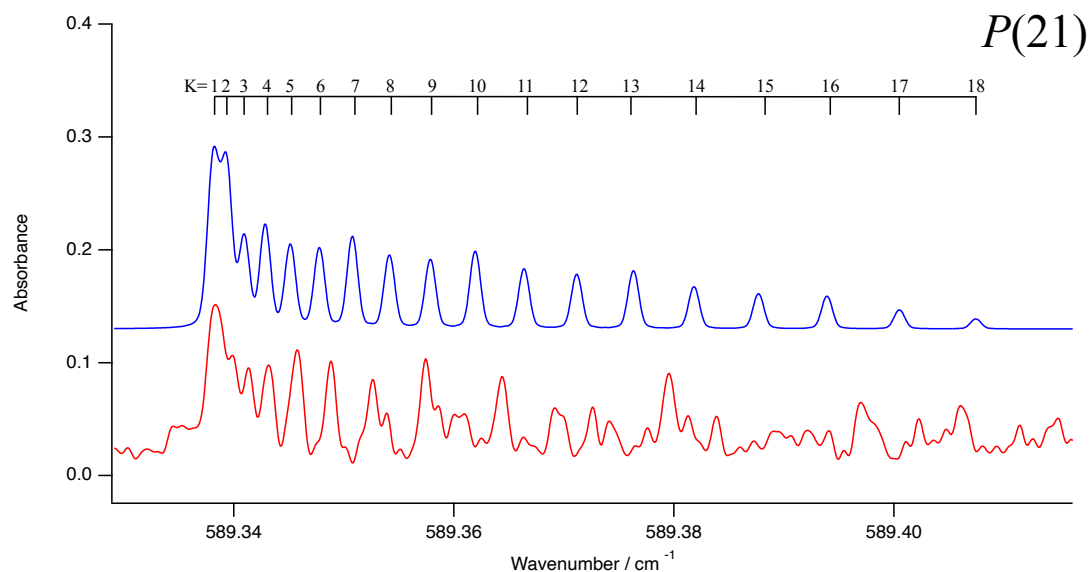


Figure 8: Zoom on the K series of $P(21)$ in the $2\nu_{20}$ band. The higher the K , the more visible the perturbations become.

way. From what we have observed, tensorial formalism is really well adapted to this type of molecule with such a symmetry. This model allows a systematic construction of all necessary operators up to any order of the development and this makes it easy to program and more flexible. Nevertheless, despite the fact we originally used this formalism to try to analyze the $2\nu_{20}$ band, it did not work better. The spectrum of the first overtone of the ν_{20} mode was recorded but analysis could not get further because of the difficulty in assigning lines in the perpendicular sub-band E . Assigning the $\nu_{20} = 2$ rovibrational states from the $2\nu_{20} \leftarrow \nu_{20}$ hot band could be of great help for going further in the analysis of the first overtone.

Acknowledgments

The authors are indebted to O. Pirali for the optical alignment and tuning of the long path absorption cell coupled to the high resolution interferometer. The authors are grateful to Soleil and the AILES staff for providing synchrotron beam under the proposal 20171389.

References

- [1] H. Cottin, M.-C. Gazeau, J.-F. Doussin, F. Raulin, An experimental study of the photodegradation of polyoxymethylene at 122, 147 and 193 nm, *Journal of photochemistry and photobiology A: Chemistry* 135 (1) (2000) 53–64.
- [2] H. Cottin, Y. Bénilan, M.-C. Gazeau, F. Raulin, Origin of cometary extended sources from degradation of refractory organics on grains: polyoxymethylene as formaldehyde parent molecule, *Icarus* 167 (2) (2004) 397–416.
- [3] T. Oka, K. Tsuchiya, S. Iwata, Y. Morino, Microwave spectrum of s-trioxane, *Bulletin of the Chemical Society of Japan* 37 (1) (1964) 4–7.

- [4] J. Bellet, J.-M. Colmont, J. Lemaire, Millimeter wave study of the ground state and several excited vibrational states of trioxane, *Journal of Molecular Spectroscopy* 34 (2) (1970) 190–205.
- [5] J. Colmont, Microwave spectrum of trioxane in four excited degenerate vibrational states, especially in the $2\nu_{20}$ (E) state and the combination state ν_7 (A_1)+ ν_{20} (E), *Journal of Molecular Spectroscopy* 58 (2) (1975) 220–228.
- [6] J. Henninot, H. Bolvin, J. Demaison, B. Lemoine, The infrared spectrum of trioxane in a supersonic slit jet, *Journal of Molecular Spectroscopy* 152 (1) (1992) 62–68.
- [7] J.-M. Colmont, Assignment method of the rotational spectrum of a slightly asymmetric molecule: application to the ^{13}C and ^{18}O species of the molecule of trioxane, *Journal of Molecular Spectroscopy* 80 (1) (1980) 166–177.
- [8] J. Gadhi, G. Wlodarczyk, D. Boucher, J. Demaison, The submillimeter-wave spectrum of trioxane, *Journal of Molecular Spectroscopy* 133 (2) (1989) 406–412.
- [9] B. M. Gibson, N. C. Koeppe, B. J. McCall, Rotationally-resolved spectroscopy of the ν_{16} band of 1, 3, 5-trioxane, *Journal of Molecular Spectroscopy* 317 (2015) 47–49.
- [10] V. Boudon, J.-P. Champion, T. Gabard, M. Loëte, M. Rotger, C. Wenger, Spherical top theory and molecular spectra, in: M. Quack, F. Merkt (Eds.), *Handbook of High Resolution Spectroscopy*, Vol. 3, John Wiley & Sons, Ltd, Chichester, 2011, Ch. 39, pp. 1437–1460.
- [11] C. Wenger, V. Boudon, M. Rotger, J. P. Sanzharov, J. P. Champion, XTDS and SPVIEW: Graphical tools for the analysis and simulation of high-resolution molecular spectra, *Journal of Molecular Spectroscopy* 251 (2008) 102–113.
- [12] T. A. Mohamed, Some periodic trends, molecular structure, normal coordinate analysis of 1, 3, 5-trioxane,-trithiane and-triselenane: computational and vibrational studies, *Journal of Molecular Structure: THEOCHEM* 713 (1-3) (2005) 179–192.
- [13] J.-B. Brubach, L. Manceron, M. Rouzieres, O. Pirali, D. Balcon, F. K. Tchana, V. Boudon, M. Tudorie, T. Huet, A. Cuisset, et al., Performance of the AILES THz-Infrared beamline at SOLEIL for High resolution spectroscopy, in: *AIP Conference Proceedings*, Vol. 1214, American Institute of Physics, 2010, pp. 81–84.
- [14] I. Smirnova, A. Cuisset, F. Hindle, G. Mouret, R. Bocquet, O. Pirali, P. Roy, Gas-phase synchrotron FTIR spectroscopy of weakly volatile alkyl phosphonate and alkyl phosphate compounds: vibrational and conformational analysis in the terahertz/far-IR spectral domain, *The Journal of Physical Chemistry B* 114 (50) (2010) 16936–16947.
- [15] V.-M. Horneman, R. Anttila, S. Alanko, J. Pietilä, Transferring calibration from CO_2 laser lines to far infrared water lines with the aid of the ν_2 band of OCS and the ν_2 , $\nu_1 - \nu_2$, and $\nu_1 + \nu_2$ bands of $^{13}\text{CS}_2$: Molecular constants of $^{13}\text{CS}_2$, *Journal of Molecular Spectroscopy* 234 (2) (2005) 238–254.
- [16] A. El Hilali, C. Wenger, V. Boudon, M. Loëte, C_{3v} top data system (C_{3v} TDS) software for spectrum simulation of XY_3Z symmetric-top molecules using the $O(3) \supset C_{\infty v} \supset C_{3v}$ group chain, *Journal of Quantitative Spectroscopy and Radiative Transfer* 111 (9) (2010) 1305–1315.
- [17] V. Boudon, J.-P. Champion, T. Gabard, M. Loëte, F. Michelot, G. Pierre, M. Rotger, C. Wenger, M. Rey, Symmetry-adapted tensorial formalism to model rovibrational and rovibronic spectra of molecules pertaining to various point groups, *J. Mol. Spectrosc.* 228 (2004) 620–634.
- [18] J.-P. Champion, M. Loëte, G. Pierre, Spherical top spectra, in: K. N. Rao, A. Weber (Eds.), *Spectroscopy of the Earth’s atmosphere and interstellar medium*, Academic Press, San Diego, 1992, pp. 339–422.
- [19] N. Cheblal, M. Loëte, V. Boudon, Development of the dipole moment and polarizability operators of octahedral molecules, *J. Mol. Spectrosc.* 197 (1999) 222–231.
- [20] A. E. Hilali, V. Boudon, M. Loëte, Spectroscopy of XY_3Z (C_{3v}) molecules: A tensorial formalism adapted to the $O(3) \supset C_{\infty v} \supset C_{3v}$ group chain, *J. Mol. Spectrosc.* 234 (2005) 113–121.
- [21] D. Papoušek, M. Aliev, *Molecular vibrational-rotational spectra*, Elsevier, New York, 1982.
- [22] A. E. Hilali, V. Boudon, M. Loëte, Development of the Hamiltonian and transition moment operators of symmetric top molecules using the $O(3) \supset C_{\infty v} \supset C_{3v}$ group chain, *J. Mol. Spectrosc.* 234 (2005) 176–181.

- [23] I. Haykal, D. Doizi, V. Boudon, A. El Hilali, L. Manceron, G. Ducros, Line positions in the $\nu_6 = 1$ band of methyl iodide: Validation of the C_{3v} TDS package based on the tensorial formalism, *Journal of Quantitative Spectroscopy and Radiative Transfer* 173 (2016) 13–19.
- [24] J. K. Watson, Simplification of the molecular vibration-rotation Hamiltonian, *Molecular Physics* 15 (5) (1968) 479–490.
- [25] Maxima, [Maxima, a computer algebra system. version 5.34.1](https://maxima.sourceforge.io/) (2014).
URL <https://maxima.sourceforge.io/>
- [26] V. Boudon, C. Richard, B. Willis, Analytical expression of tensorial rotational operators for semi-classical interpretation of molecular spectra. Relations between molecular Hamiltonian parameters in different formalisms., *Journal of Molecular Spectroscopy*(submitted) (2022).
- [27] C. M. Western, Pgopher: A program for simulating rotational, vibrational and electronic spectra, *Journal of Quantitative Spectroscopy and Radiative Transfer* 186 (2017) 221–242.
- [28] H. Pickett, The fitting and prediction of vibration-rotation spectra with spin interactions, *J. Mol. Spectrosc.* 148 (1991) 371–377.
- [29] H. Klein, S. Belov, G. Winnewisser, Terahertz spectrum of trioxane, *Zeitschrift für Naturforschung A* 51 (1-2) (1996) 123–128.
- [30] J. Colmont, Étude en ondes millimétriques des variétés isotopiques en ^{13}C et ^{18}O de la molécule de trioxane: Structure de la molécule, *Journal of Molecular Structure* 21 (3) (1974) 387–396.